Journal of Beijing Institute of Technology, 2025, Vol. 34, No. 3

Direct Signal Interference Suppression in DVB-S Based on Passive Bistatic Radar

Jianyu He, Hongwen Yu✉, Zhichao Sheng, Yong Fang
(School of Communication and Information Engineering, Shanghai University, Shanghai 200444, China)

Abstract: Passive bistatic radar (PBR) frequently experiences interference from direct signal waves when detecting maritime targets, which can completely mask target echoes, particularly for distant targets or weak targets with low radar cross-section (RCS). To mitigate this, the paper proposes a direct signal interference (DSI) suppression method. The approach involves dual-channel reception of digital video broadcast satellites (DVB-S) signals from the China Sat-9, followed by signal preprocessing. The reference and surveillance channel signals are then segmented. After segmentation, the signals undergo fast Fourier transformation (FFT), and an adaptive filtering clutter suppression method is applied at each frequency point. Finally, an inverse fast Fourier transform (IFFT) is performed on the suppressed signals to obtain the DSI-suppressed output. Compared to traditional clutter suppression techniques, this method is not only faster but also achieves more effective suppression. Simulation experiments involving both single and multiple targets validate the superiority of the proposed algorithm.

Keywords: passive bistatic radar (PBR); direct signal interference (DSI); digital video broadcast satellite (DVB-S)

1 Introduction

Passive bistatic radar (PBR) systems [1] commonly utilize digital video broadcast satellites (DVB-S) [2–3], digital video broadcasting–terrestrial (DVB-T) [4], global navigation satellite systems (GNSS) [5–6], global positioning system (GPS) [7], BeiDou navigation satellite system (BDS) [8–9], frequency modulation (FM) radio broadcasting [10] and other opportunistic sources as illuminators for target detection. These systems have garnered significant research attention in recent decades due to their extensive coverage, low operational cost and environmental sustainability. A typical PBR system includes a reference channel that directly captures signals from the satellite, and a surveillance channel that is directed towards the target area to detect responses from all objects within the antenna's coverage. In ideal conditions, the reference channel collects a delayed version of the clean transmitted signal, which signal is then correlated with the surveillance signal to generate a three-dimensional range-Doppler (RD) map containing target information. However, However, the ideal model rarely holds in real-world, particularly for systems using satellites as illuminators.

The surveillance signal typically includes direct signal interference (DSI), comprising direct wave signals, multipath interference, and clutter reflections. The presence of these interferences obscures the extraction of target information from the three-dimensional RD map. Conse-

Manuscript received Jan. 18, 2025; revised Feb. 19, 2025; accepted Mar. 1, 2025. The associate editor coordinating the review of this manuscript was Dr. Yixiao Gu. The work was supported in part by Shanghai Sailing Scholar (No. 23YF1412700) and in part by the Key Laboratory Innovation and Development Fund Project, China (No. 61424132006).
✉ Corresponding author. Email: hw_yu@shu.edu.cn
DOI: 10.15918/j.jbit1004-0579.2025.002

quently, DSI suppression is essential for effective target detection in PBR systems and remains a significant challenge in the field.

Over the years, methods for suppressing DSI in PBR systems have primarily included spatial filtering and adaptive filtering techniques. In [11], a spatial filtering approach was proposed to suppress the direct path and multipath interference generated by single-frequency networks (SFN). This method effectively reduces DSI in digital terrestrial television broadcasting (DTTB) systems, though its clutter suppression performance in the target direction requires further improvement.

Recently, adaptive filtering methods have gained widespread use in DSI suppression due to their advantages, including strong interference resistance and high robustness. In [12], the application of Wiener filtering to mitigate clutter in wideband radar echoes has facilitated the enhancement of target detection capabilities. However, the efficacy of this approach is contingent upon the precision of the radar transmission signal and scatterer characteristic modeling. The least mean squares (LMS) algorithm, celebrated for its computational simplicity, asymptotically converges to the optimal Wiener solution under stationary environmental conditions [13–14] applied the LMS algorithm for DSI suppression, but due to its inherent limitations, researchers have developed newer techniques to replace it [15–16], with normalized LMS (NLMS) [17] and variable step-size LMS (VSLMS) [18] being notable examples. [19] extended the traditional one-dimensional NLMS filter to a two-dimensional structure, incorporating both time and doppler frequency to more effectively suppress strong multipath components and target echoes. By controlling the sparsity of the filter weights using a two-dimensional matrix, the detection capability for weak targets was significantly enhanced. In [20], a comparative analysis of clutter suppression performance between the NLMS and recursive least squares (RLS) algorithms revealed that while the RLS algorithm exhibits faster convergence, its computational complexity significantly exceeds that of the NLMS. Consequently, the NLMS algorithm is often favored in radar system applications. The CLEAN algorithm, originally developed for deconvolution in radio interferometry to improve image quality, was later adapted to radar for clutter suppression [21].

However, due to its stringent requirements on signal characteristics, it is rarely used in satellite-based bistatic systems. Nonetheless, apart from adaptive filtering methods, segmenting the received signal is a common approach in PBR systems, with techniques such as extensive cancellation algorithm (ECA) [22], ECA-batches (ECA-B) [23] and ECA-sliding (ECA-S) [24]. This method enhances algorithm performance while reducing system resource consumption. It highlights that the ECA algorithm requires estimating filter weights over the entire coherent processing interval (CPI), which can lead to adaptive losses in non-stationary environments, negatively impacting the detection of slow-moving targets in [22]. While ECA-B enhances the system's adaptability to time-varying environmental conditions and reduces computational complexity, it may inadvertently eliminate some target echoes. Conversely, the ECA-S enhances the detection of slow-moving targets. The parallel implementation of the ECA algorithm was reexamined from a maximum likelihood standpoint, with a focus on partitioning the reference and surveillance channels to enhance the efficiency of parallel processing [25].

To overcome the limitations of traditional methods, such as high algorithmic complexity and the loss of certain echo information, our primary focus is on designing an algorithm that minimizes system resource consumption while retaining complete target information. The proposed method segments the signals collected by the PBR system and then transforms them into the frequency domain for clutter suppression.

The performance of this algorithm will be compared against traditional algorithms using simulated DVB-S signals. The algorithms considered for comparison are

1) Least mean squares (LMS);
2) Normalized least mean squares (NLMS);
3) Recursive least squares (RLS);
4) Extensive cancellation algorithm (ECA).

The DVB-S signal examined in this paper is specified by the industry standard GY/T 233-2008, issued by the State Administration of Radio, Film, and Television, and covers 98% of mainland China. The signal utilizes quadrature phase shift keying (QPSK) modulation, enabling individual reception. However, it is crucial to ensure the purity of the reference channel making the preprocessing of the reference signal essential before performing DSI suppression. The contributions of this study are as follows:

1) Unlike traditional time-domain segmentation techniques, a mehod is proposed to segments the signal and then converts it into the frequency domain for clutter suppression at individual frequency points, resulting in more versatile signal processing.

2) Compared to traditional adaptive filtering algorithms, the proposed method significantly reduces complexity while enhancing target detection performance.

The rest of this paper is organized as follows: Section 2 analyzes the bistatic system model in terms of signal, power, and processing. Section 3 provides a detailed explanation of the proposed algorithm's processing steps. Section 4 examines the results of different processing algorithms in single and multiple target scenarios, presenting performance comparison methods and runtime metrics. Finally, Section 5 concludes the paper.

2 Bistatic Passive Radar Signal Model

In this section, we present a summary of the fundamental BPR signal model. Subsequently, power analysis is conducted in accordance with the bistatic relationship, and the principle of RD processing is elaborated. These discussions establish a solid foundation for addressing the challenge of DSI suppression.

2.1 PBR Received Siganl Model

The configuration diagram of the DVB-S based bistatic passive radar is shown in Fig. 1. It comprises a transmission source, two receiving antennas and a sea surface target. The transmission source is China Sat-9, operating in the Ku band, with parameters provided in Tab. 1. The receiving antennas are labeled as the reference antenna and the surveillance antenna. The reference antenna is oriented toward the satellite to capture the direct signal as a reference, while the surveillance antenna is directed toward the tar-

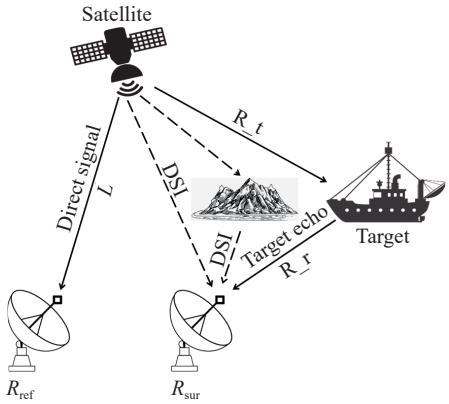

Fig. 1 Configuration diagram of the DVB-S-based bistatic passive radar

Tab. 1 China Sat-9 parameters

Parameters	Value
Location	92.2°E
Band	Ku
Bandwidth	54 MHz
Transmit power	10700 W
EIRP	46 –56 dBW
Uplink frequencies	12.75 –14.50 GHz
Downlink frequencies	10.70 –12.75 GHz
Modulation mode	QPSK
Carrier frequency	12.06 GHz
Sampling frequency	100 MHz
Symbol rate	28.8 MHz

get to collect the signal reflected from the object of interest. However, the surveillance antenna often also receives the direct signal from the satellite, echoes from nearby static islands, and other interference signals.

The signal received by the reference antenna can be represented as

$$s_{\text{ref}}(n) = As(n) + w_{\text{ref}}(n) \tag{1}$$

where $n = 1, 2, \cdots, N$ and N denotes the length of the direct signal, A represents the complex amplitude of the transmitted waveform, and $s(n)$ refers to the direct signal. The term $w_{\text{ref}}(n)$ accounts for additive white Gaussian noise.

Despite employing highly directional methods during signal acquisition to maximize the SNR, the reference signal often contains clutter originating from the transmission channel. This clutter introduces false peaks on the RD surface, potentially leading to target misidentification. To mitigate these effects, it is essential to reconstruct the collected reference signal, eliminating clutter, multipath interference, and noise. However, this reconstruction process is computationally intensive, and the carrier phase effect must be accurately addressed to prevent performance degradation during matched filtering. Furthermore, proper signal demodulation prior to reconstruction is necessary to further enhance the SNR.

The signal received by the surveillance antenna typically consists of DSI, target echoes and thermal noise, which can be expressed as

$$s_{\text{sur}}(n) = s_{\text{DSI}}(n) + s_{\text{target}}(n) + w_{\text{sur}}(n) \tag{2}$$

where $s_{\text{sur}}(n)$ represents the received surveillance signal, $s_{\text{DSI}}(n)$ denotes the direct signal component, while $s_{\text{target}}(t)$ represents the target echo, which is the signal reflected from the target, $w_{\text{sur}}(n)$ corresponds to thermal noise. Both the DSI and target components consist of scattered signals from $s_{\text{ref}}(n)$. By accounting for the doppler effect resulting from the target's motion and the time delay introduced by the target's distance, (2) can be reformulated as follows

$$\begin{aligned} s_{\text{sur}}(n) = &\sum_{q=1}^{Q} A_q s(n - d_q) + \\ &\sum_{u=1}^{U} A_u s(n - d_u) \mathrm{e}^{\mathrm{j}2\pi f_u \frac{n}{f_s}} + w_{\text{sur}}(n) \end{aligned} \tag{3}$$

where A_q and d_q are the complex amplitude and the delay of the qth $(q = \{1, 2, \cdots, Q\})$ DSI, respectively. A_u, d_u and f_u are the complex amplitude, the delay and the doppler frequency of the uth $(u = \{1, 2, \cdots, U\})$ target echo. f_s is the sampling rate.

The purpose of DSI suppression is to accurately reconstruct the direct signal, thereby enabling the extraction of its transmission properties and facilitating the estimation of the first two terms in (3) using suitable methodologies. Subsequently, coherent processing is applied to subtract the estimated DSI component from the received surveillance signal, leaving behind the residual target information and noise. This approach improves the accuracy of target detection by minimizing interference from the direct signal.

2.2 Power Analysis

In PBR systems, conducting a power analysis is a crucial step to ascertain the detectability of the target signal. Typically, this analysis involves modeling the target power by employing the bistatic radar equation, which is

$$\text{SNR} = \frac{P_t G_t}{(4\pi)^2 R_1^2 R_2^2} \sigma_\theta \frac{G_r \lambda^2}{4\pi} \frac{B_s T_a}{T_p L_s} \tag{4}$$

where P_t and G_t are the transmission power and antenna gain of the China Sat-9, respectively, R_1 and R_2 are the distance from the satellite to the receiver and distance from the target to the receiver, respectively, σ_θ is the radar cross section (RCS) of the target, G_r is the gain of surveillance antenna, $\lambda = c/f_s$ is the wavelength, B_s is the signal bandwidth, T_a is the accumulation duration, L_s is the system loss, $T_p = kT$ is the power of the system noise, k is the Boltzmann's constant, and T is the system noise temperature.

Enhancing the SNR is pivotal for improving

radar target detection capabilities, particularly in complex environments. When fixing parameters of the DVB-S system and establishing the target distance, it is contributed to increase the SNR by increasing the RCS, reducing the system's inherent thermal noise, and effectively suppressing DSI.

2.3 Bistatic Passive Radar Processing

In PBR, the computation of the RD map is fundamental for enabling target detection and tracking. According to the reference signal and the surveillance signal, RD processing is achieved through the cross-ambiguity function calculation, which is as follows

$$\chi(\tau, f_d) = \int_{-T/2}^{T/2} S_{\text{ref}}(t) S_{\text{sur}}^*(t-\tau) \mathrm{e}^{-\mathrm{j}2\pi f_d t}\, \mathrm{d}t \qquad (5)$$

where τ is the ratio of the target's bistatic range R_d to the speed of light c, which is the time delay information of the target, R_d can be viewd as $R_d = R_t + R_r - L$, and R_t, R_r, L represent the distances from the transmitter to the receiver, the transmitter to the target, and the target to the receiver, respectively. f_d is the doppler frequency, $(\cdot)^*$ denotes complex conjugation. Fig. 2 is the example of RD maps for DVB-S signals.

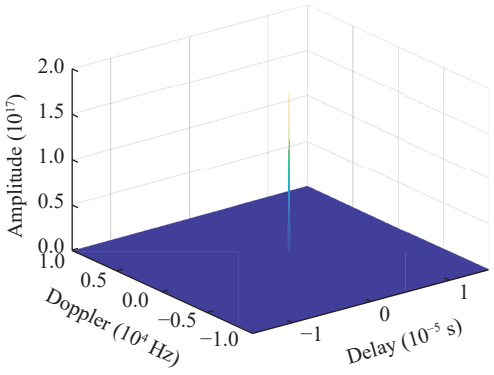

Fig. 2 RD maps for DVB-S signals

DSI processing diminishes the power of the direct signal, thereby enhancing the discernibility of the target's peak. Consequently, it is essential to perform DSI processing prior to RD mapping. Moreover, the intrinsic Doppler processing in RD formation aids in further isolating the echoes of moving targets from stationary clutter and direct signal components. This separation is facilitated by the fact that the auto-correlation of the noise-like digital waveform reaches a minimum at $10\lg(\tau B)$ dB, which is situated below the peak at zero delay and Doppler [26].

3 Proposed DSI Suppression Scheme

In this section, we describe a signal processing scheme that leverages signals from both the reference and surveillance channels to eliminate clutter and facilitate target detection. Fig. 3 illustrates the architecture of the proposed signal processing approach. To further reduce clutter, multipath interference, and noise within the reference channel, a preprocessing scheme, as proposed in [23], is implemented. In PBR systems, the reference signal is initially demodulated using a standard DVB-S demodulator to produce an error-free copy of the transmitted data. This modulated signal is then compared with the original reference signal to identify any subtle phase offsets or drifts between the local oscillators of the PBR receiver and transmitter. Based on the estimated phase offsets, the error-free digital data is reconstructed. This regenerated reference signal is subsequently utilized for clutter cancella-

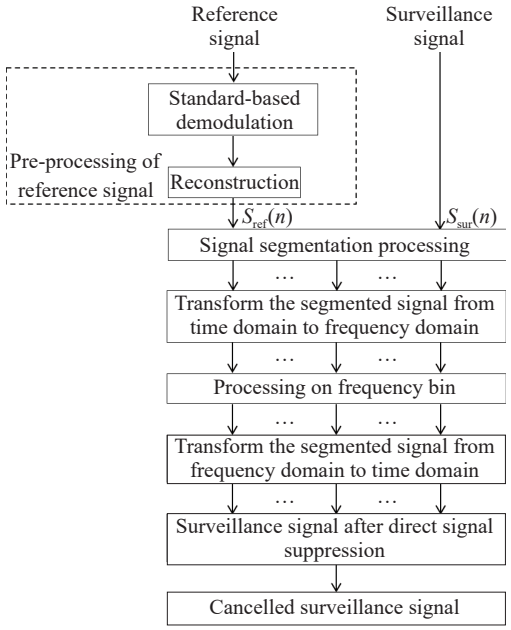

Fig. 3 Sketch of the proposed DSI suppression scheme

tion and target detection in the surveillance signal. The detailed contents will be discussed in this section.

The proposed DSI suppression method consists of several key steps, outlined as follows.

Initially, both the surveillance signal and the preprocessed reference signal are segmented into multiple short intervals. These segmented signals are then transformed from the time domain to the frequency domain. The strong correlation between the reference signal and multipath clutter is recognized at identical frequencies. To recoganize the weak correlation between the reference signal and the target echo signal, an adaptive filter with estimated weights is applied in the frequency domain. This filter is specifically designed to mitigate direct wave signal interference in the surveillance signal, thereby effectively reducing clutter at each frequency point. Finally, the clutter-suppressed signals in the frequency domain are reconverted into the time domain. The process of segmentation and subsequent steps is depicted in Fig. 4.

Traditional clutter suppression methods are often hindered by high computational complexity. The algorithm presented in this paper addresses this issue by employing block processing techniques for signal processing. Furthermore, the introduction of partial overlap processing of the surveillance signal enhances the smoothness of the filter's output. The specific methodology is detailed as follows:

Step 1: The reference and surveillance signals are segmented into m segments, where the ith segment $(i = 0,1,\cdots,m\text{-}1)$ of the signal is presented as follows

$$\begin{cases} R(i) = [s_{\text{ref}}(il_{\text{step}}+1), s_{\text{ref}}(il_{\text{step}}+2), \cdots, \\ \qquad \cdots, s_{\text{ref}}(il_{\text{step}}+l_{\text{seg}})]^{\text{T}} \\ S(i) = [s_{\text{sur}}(il_{\text{step}}+1), s_{\text{sur}}(il_{\text{step}}+2), \cdots, \\ \qquad \cdots, s_{\text{sur}}(il_{\text{step}}+l_{\text{seg}})]^{\text{T}} \end{cases} \tag{6}$$

where $[\cdot]^{\text{T}}$ denotes transpose, the length of each segemented signal is $l_{\text{seg}} = n/m$, $l_{\text{step}} = l_{\text{seg}}/2$ is the partial of overlap.

Step 2: The segmented signals undergo transformation from the time domain to the frequency domain. The results of the FFT applied to these signals are represented as follows:

$$R_i(k\Delta f) = \text{FFT}[As_i(n)] + W_{\text{ref}}(k\Delta f) \tag{7}$$

$$\begin{aligned} S_i(k\Delta f) = &\sum_{q=1}^{Q} \text{FFT}[A_q s(n-d_q)] + \\ &\sum_{u=1}^{U} \text{FFT}[A_k s(n-d_k) \text{e}^{\text{j}2\pi f_k \frac{n}{f_s}}] + \\ &W_{\text{sur}}(k\Delta f) \end{aligned} \tag{8}$$

where $R_i(k\Delta f) = [R_{i,1}, R_{i,2}, \cdots, R_{i,k}, \cdots, R_{i,l_{\text{seg}}}]$, $R_{i,k}$ is the complex value for $R(i)$ in the kth frequency bin, $\Delta f = f_s/l_{\text{seg}}$ is the interval between frequency bins, $W(k\Delta f)$ represents spectrum of noise for different signals.

After undergoing FFT, the segmented reference signals are represented as follows

$$\boldsymbol{R} = \begin{bmatrix} \boldsymbol{R}_1 & \cdots & \boldsymbol{R}_k & \cdots & \boldsymbol{R}_{l_{\text{seg}}} \end{bmatrix} = \begin{bmatrix} R_{1,1} & \cdots & R_{1,k} & \cdots & R_{1,l_{\text{seg}}} \\ \vdots & \ddots & \vdots & \ddots & \vdots \\ R_{m,1} & \cdots & R_{m,k} & \cdots & R_{m,l_{\text{seg}}} \\ \vdots & \ddots & \vdots & \ddots & \vdots \\ R_{2m,1} & \cdots & R_{2m,k} & \cdots & R_{2m,l_{\text{seg}}} \end{bmatrix} \tag{9}$$

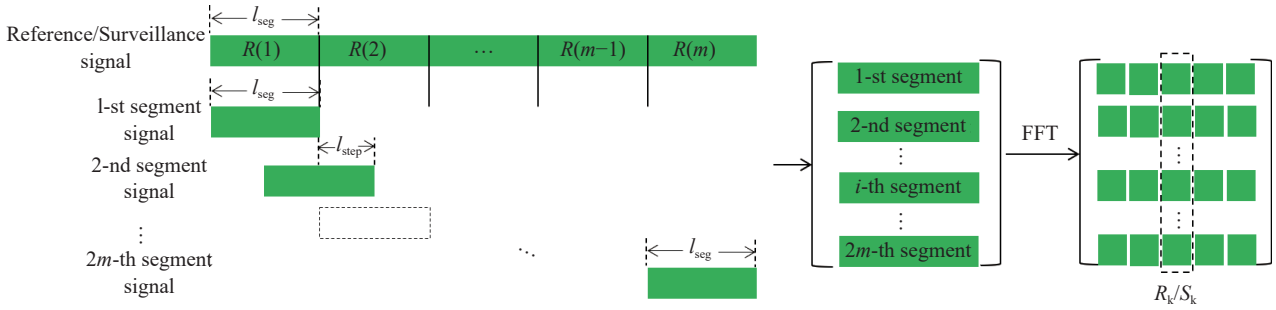

Fig. 4 Diagram of signal segment processing

After undergoing FFT, the segmented surveillance signals are represented as

$$\boldsymbol{S}=\left[\boldsymbol{S}_1 \quad \cdots \quad \boldsymbol{S}_k \quad \cdots \quad \boldsymbol{S}_{l_{\text{seg}}}\right]= \begin{bmatrix} S_{1,1} & \cdots & S_{1,k} & \cdots & S_{1,l_{\text{seg}}} \\ \vdots & \ddots & \vdots & \ddots & \vdots \\ S_{m,1} & \cdots & S_{m,k} & \cdots & S_{m,l_{\text{seg}}} \\ \vdots & \ddots & \vdots & \ddots & \vdots \\ S_{2m,1} & \cdots & S_{2m,k} & \cdots & S_{2m,l_{\text{seg}}} \end{bmatrix} \tag{10}$$

Step 3: In the clutter suppression process across the signal bandwidth, a clutter spatial sub-matrix is constructed, and filter weight coefficients are estimated for each frequency point. Subsequently, the surveillance signal which after clutter suppression is obtained and aggregated for output. The process for each frequency bin is illustrated in Fig. 5, with specific calculations as follows

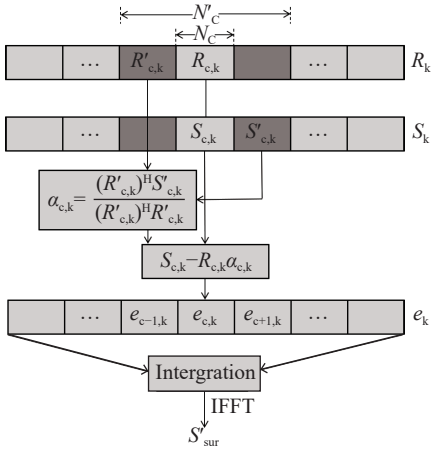

Fig. 5 The diagram of the process on frequency bin

1) The signal $\boldsymbol{S}_k$ and $\boldsymbol{R}_k$ are divided into C batches, and the number of each batch is $N_C=2\,m/C$. The cth $(c=\{0,1,2,\cdots,C-1\})$ batch surveillance signal on the kth frequency bin is written as

$$\boldsymbol{S}_{c,k}=[S_{cN_C+1,k},S_{cN_C+2,k},\cdots,S_{(c+1)N_C,k}]^{\mathrm{T}} \tag{11}$$

2) The clutter subspace matrix constructed from the cth batch of reference signal on the kth frequency bin is written as

$$\boldsymbol{R}_{c,k}=[R_{cN_C+1,k},R_{cN_C+2,k},\cdots,R_{(c+1)N_C,k}]^{\mathrm{T}} \tag{12}$$

3) Estimate the filter weight coefficient, which is expressed as

$$\alpha_{c,k}=\frac{(\boldsymbol{R}'_{c,k})^{\mathrm{H}}\boldsymbol{S}'_{c,k}}{(\boldsymbol{R}'_{c,k})^{\mathrm{H}}\boldsymbol{R}'_{c,k}} \tag{13}$$

where $(\cdot)^{\mathrm{H}}$ denotes complex conjugate transpose, $\alpha_{c,k}$ is the filter weight coefficient, $\boldsymbol{R}'_{c,k}$ and $\boldsymbol{S}'_{c,k}$ are the cth batch of reference and surveillance signal, respectively,which are expressed as

$$\begin{aligned}\boldsymbol{S}'_{c,k}=&[S_{cN'_C+1+N_s,k},S_{cN'_C+2+N_s,k},\\&\cdots,S_{(c+1)N'_C+N_s,k}]^{\mathrm{T}}\end{aligned} \tag{14}$$

$$\begin{aligned}\boldsymbol{R}'_{c,k}=&[R_{cN'_C+1+N_s,k},R_{cN'_C+2+N_s,k},\\&\cdots,R_{(c+1)N'_C+N_s,k}]^{\mathrm{T}}\end{aligned} \tag{15}$$

where $N_s=(N'_C-N_C)/2$, N'_C is the length of signal $\boldsymbol{S}'_{c,k}$.

4) Filter out the clutter in the surveillance signal $S_{c,k}$

$$\boldsymbol{e}_{c,k}=\boldsymbol{S}_{c,k}-\boldsymbol{R}_{c,k}\alpha_{c,k} \tag{16}$$

where $\boldsymbol{e}_{c,k}$ is the surveillance signal after filtering out the clutter. And Eq. (16) can be expressed in detail as

$$\boldsymbol{e}_{c,k}=\begin{bmatrix} e_{0,k} & e_{C,k} & \cdots & e_{C(N_c-1),k} \\ \vdots & \vdots & \ddots & \vdots \\ e_{c,k} & e_{C+c,k} & \cdots & e_{C(N_c-1)+c,k} \\ \vdots & \vdots & \ddots & \vdots \\ e_{C-1,k} & e_{2C-1,k} & \cdots & e_{CN_c,k} \end{bmatrix} \tag{17}$$

The segmented surveillance signals after clutter suppression are represented as

$$\boldsymbol{e}=\left[\boldsymbol{e}_1 \quad \cdots \quad \boldsymbol{e}_k \quad \cdots \quad \boldsymbol{e}_{l_{\text{seg}}}\right]= \begin{bmatrix} e_{1,1} & \cdots & e_{1,k} & \cdots & e_{1,l_{\text{seg}}} \\ \vdots & \ddots & \vdots & \ddots & \vdots \\ e_{m,1} & \cdots & e_{m,k} & \cdots & e_{m,l_{\text{seg}}} \\ \vdots & \ddots & \vdots & \ddots & \vdots \\ e_{2m,1} & \cdots & e_{2m,k} & \cdots & e_{2m,l_{\text{seg}}} \end{bmatrix} \tag{18}$$

where $\boldsymbol{e}_k$ is the integrated signal expression of $\boldsymbol{e}_{c,k}$.

5) The segmented signals are transformed from the frequency domain to the time domain. The IFFT result of signal is represented as

$$s'_{sur}(n)=\mathrm{IFFT}[\boldsymbol{e}] \tag{19}$$

The main processe of the proposed DSI surppression algorithm is shown in Algorithm 1.

Algorithm 1 The main processe of the proposed method.

input: Original surveillance signal $s_{\text{sur}}(n)$ and reference signal $s_{\text{ref}}(n)$, sampling frequency f_{s}.

output: Surveillance signal $s'_{\text{sur}}(n)$ after DSI suppression

$s'_{\text{sur}}(n) \leftarrow \text{zeros}(1, \text{length}(s_{\text{ref}}(n)))$; $l_{\text{seg}} \leftarrow \text{length}(s_{\text{ref}}(n))/m$; $l_{\text{step}} \leftarrow \lfloor l_{\text{seg}}/2 \rfloor$;

for $i \leftarrow 1$ **to** m **do**

  Perform the signal segment process for the $s_{\text{sur}}(n)$ and $s_{\text{ref}}(n)$;

  Apply the FFT to the segmented signals from time domain to frequency domain; **for** $k \leftarrow 1$ **to** l_{seg} **do**

    $\alpha_{c,k} \leftarrow \text{zeros}(1, l_{\text{seg}})$;

    $\alpha_{c,k} \leftarrow (\boldsymbol{R}'_{c,k})^H \boldsymbol{S}'_{c,k} / ((\boldsymbol{R}'_{c,k})^H \boldsymbol{R}'_{c,k})$;

    $\boldsymbol{e}_{c,k} \leftarrow \boldsymbol{S}_{c,k} - \boldsymbol{R}_{c,k}\alpha_{c,k}$;

$s'_{\text{sur}}(n) \leftarrow \text{IFFT}[\boldsymbol{e}]$;

4 Experimental Analysis

In this section, LMS, NLMS, RLS, ECA and proposed alogrithm are used to supress clutter, and then the RD map is calculated. The performance of the proposed algorithm is compared with other methods through the peak-to-floor (PFR) ratio, which is shown as

$$\text{PFR} = 10\lg\left[\frac{\text{Max}(\chi^2(\tau, f_d))}{E(\chi(\tau', f_d))}\right] \tag{20}$$

where $\chi(\tau', f_d)$ is the part of the clutter-noise floor, $E(\cdot)$ is the mean level of the clutter-noise floor.

In order to conduct comparative experiments on a single target and multiple targets with different velocities and different RCS, this paper also employs the method introduced in the second section, namely RD processing, to display the targets on the RD three-dimensional spectrum. In this simulation, the DVB-S signal is used as the transmission source, the parameters of the PBR system are shown in Tab. 1. To facilitate comparative experiments involving a single target and multiple targets with varying velocities and RCS, this study employs the RD processing method introduced in Section 2. This approach enables visualization of the targets on a three-dimensional RD spectrum. The RD processing results without DSI suppression are depicted in Fig. 6. The three-dimensional RD map is illustrated in Fig. 6(a), and the section corresponding to time delay is displayed in Fig. 6(b). Significantly, the spike observed at a Doppler frequency of 0 Hz and a time delay of 0 s represents the peak of DSI. This indicates that, at this point, the energy of the direct wave signal greatly surpasses that of the target. Consequently, this overwhelming signal strength obscures any detectable target-related information.

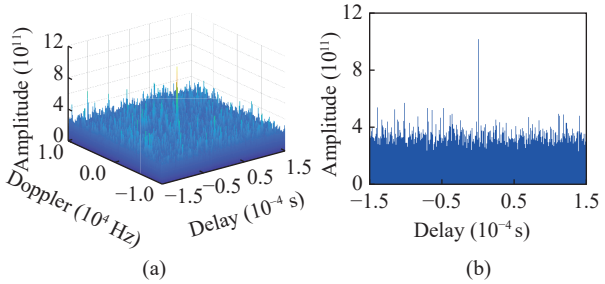

Fig. 6 RD processing for the simulation before DSI suppression: (a) RD map with 3-dimension; (b) before DSI suppression in the time delay dimension

4.1 Sigle Target Simulation

In this simulation experiment, a single target is simulated with a target velocity $v_b = 10$ m/s, a target RCS $\sigma_\theta = 21$ dBsm, and a target range $R_d = 20$ km. The corresponding time delay is 6.67×10^{-5} s, and the Doppler frequency is 803 Hz. The calculation formulas are as follows

$$\tau = \frac{R_d}{c} \tag{21}$$

$$f_d = \frac{2v_b}{\lambda}\cos(\beta/2) \tag{22}$$

where c is the speed of light, λ is the wavelength, β is the bistatic angle.

The PFR value post RD processing without DSI suppression is 14.87 dB, whereas the PFR value following DSI suppression is reduced to 12 dB. The parameters for different methods are detailed in Tab. 2. The DVB-S signal serves as the transmission source.

Tab. 2 Parameters of different method

Methods	Parameters
LMS	The order of filter is 128 and the step size is 0.01
NLMS	The order of filter is 128 and the step size is 0.01
RLS	Initialize the inverse correlation matrix factor $\delta = 13^{-}$, the order of filter is 50 and the forgetting factor is 0.99
ECA	The number of expansion units is 50
proposed	$l_{\text{seg}} = 5\,000, l_{\text{step}} = 2\,500, m = 10$

Despite the same target parameters, conventional methods such as LMS, NLMS, RLS, and ECA fail to effectively suppress DSI and detect the target. This is primarily due to their inherent limitations in adapting to non-stationary environments and their inability to precisely suppress strong interference components without losing target information. The LMS and NLMS algorithms, while computationally efficient, struggle with fast adaptation to rapidly changing interference patterns. Their performance is highly dependent on the step size parameter, which often leads to a trade-off between convergence speed and stability. The RLS algorithm, although offering faster convergence, suffers from high computational complexity and sensitivity to initial conditions and the forgetting factor. The ECA algorithm, on the other hand, may inadvertently eliminate target echoes, especially for weak targets, due to its focus on canceling dominant interference components.

In contrast, proposed method demonstrates effective suppression of DSI and successful detection of the target. This is attributed to the combination of signal segmentation, frequency-domain processing, and adaptive filtering. By transforming the signals into the frequency domain, this method can exploit the strong correlation between the reference signal and the interference components at each frequency point, leading to more precise and effective suppression. The adaptive filter applied at each frequency point dynamically adjusts its weights based on the local signal characteristics, ensuring robustness to varying interference patterns. Additionally, segmenting the signals into multiple short intervals with partial overlap allows our method to capture dynamic changes in the interference more effectively, reducing the risk of losing target information. The DSI suppression results for the single target in the RD map with three-dimensional and time delay dimensions via different methods are displayed in Fig. 7 and Fig. 8, respectively. Notably, Fig. 7(e) and Fig. 8(e) illustrate the effectiveness of the proposed method, which clearly identifies the target information with a Doppler shift of 803 Hz and a corresponding time delay of 6.67×10^{-5} s, aligning with the predefined target parameters.

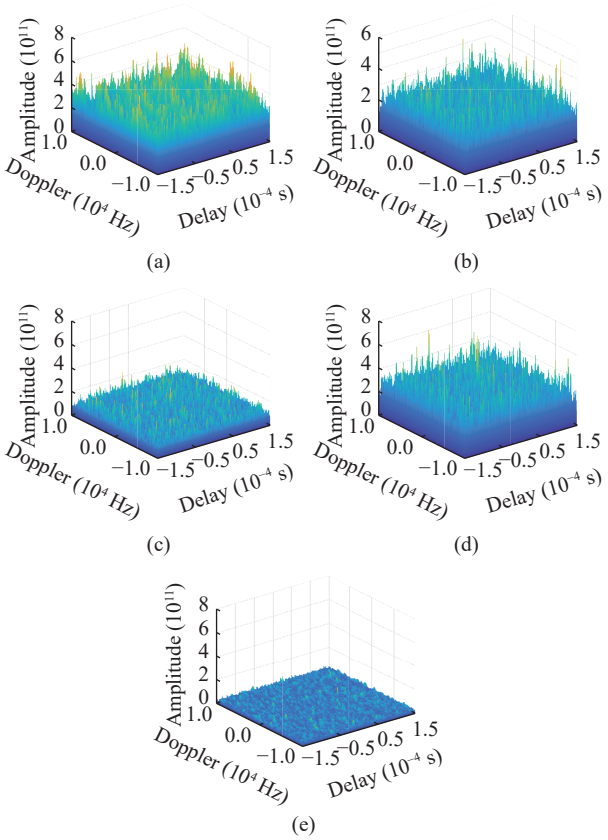

Fig. 7 DSI suppression result for sigle target in RD map with 3-dimension via diffrent methods: (a) LMS; (b) NLMS; (c) RLS; (d) ECA; (e) proposed method

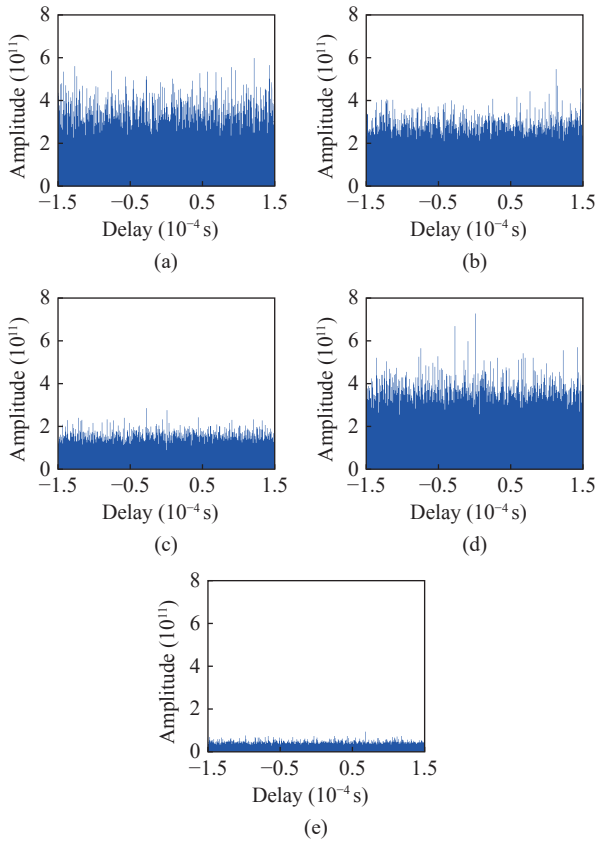

Fig. 8 DSI suppression result for sigle target in RD map with time delay dimension via diffrent methods: (a) LMS; (b) NLMS; (c) RLS; (d) ECA; (e) proposed method

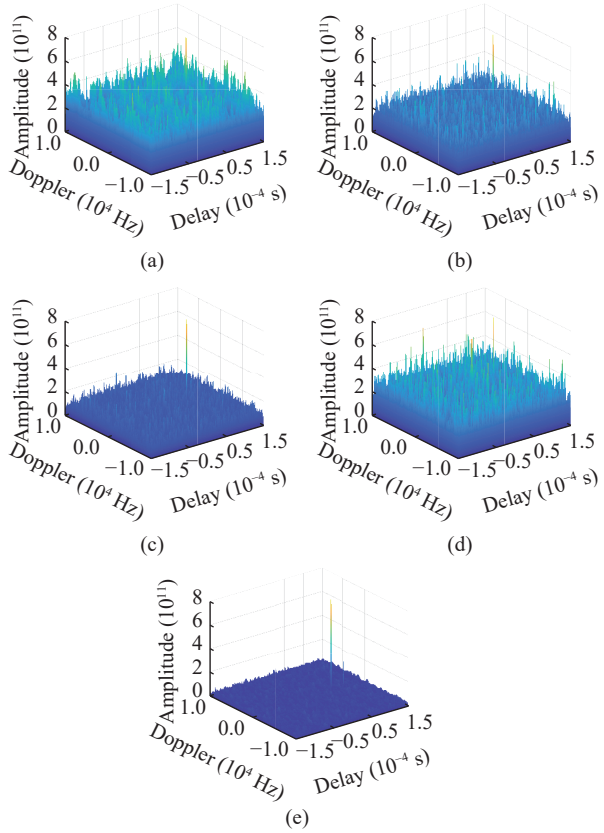

Fig. 9 DSI suppression result for sigle target in RD map with 3-dimension via diffrent methods: (a) LMS; (b) NLMS; (c) RLS; (d) ECA; (e) proposed method

4.2 Multiple Target Simulation

In this section, the DSI suppression ability for multiple targets via proposed method is evaluated. The simulation parameters for the PBR system are detailed in Tab. 1, and the motion parameters for the two targets are presented in Tab. 3. The results of DSI suppression for multiple targets in the three-dimensional RD map using different methods are displayed in Fig. 9, and the corresponding results in the time delay dimension are shown in Fig. 10. Specifically, Fig. 9(e) and Fig. 10(e) illustrate the effectiveness of the proposed method, which clearly captures the targets information. A Doppler shift of 804 Hz and a corresponding time delay of 6.67×10^{-5} s are observed for Target A, and a doppler shift of 402 Hz with a corresponding time delay of 1×10^{-4} s are observed for Target B, both aligning accurately with the predefined target parameters.

Tab. 3 Simulation parameters

Motion parameters	Target A	Target B
Range (km)	20	30
RCS (dBsm)	30	24.8
Bistatic velocity (m/s)	10	5

By comparing the PFR of different segments, the average noise floor lower than the target peak can be regarded as a successful detection, so the LMS, NLMS, and RLS methods successfully detect Target A but failed to detect Target B, which possesses a smaller RCS. The algorithm proposed in this paper demonstrates superior performance, as illustrated in the Fig. 10(e), where the peak information distinctly identifies both Target A and Target B. The peak correlates with Target A is larger than that with Target B, aligns with the parameters detailed in Tab. 3.

4.3 Result Analysis

The upward trend in Fig. 11, showing increasing

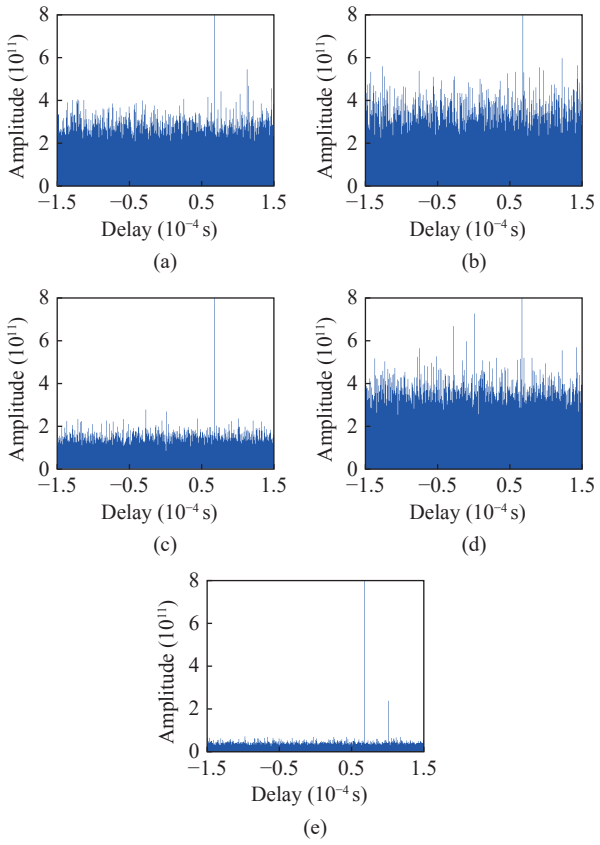

Fig. 10 DSI suppression result for sigle target in RD map with time delay dimension via diffrent methods: (a) LMS; (b) NLMS; (c) RLS; (d) ECA; (e) proposed method

PFR values with segment index, initially appears to indicate performance degradation. However, this trend is driven by the non-stationary nature of the signals, particularly from DVB-S, causes interference and target signal properties to vary over time. This leads to higher PFR values in later segments due to cumulative effects of multipath and clutter. Additionally, the dynamic interference environment changes significantly during signal capture, resulting in more pronounced interference components as processing progresses. In conclusion, the upward trend in Fig. 11 reflects the dynamic nature of the signal and interference environment, rather than performance degradation. The initial increase in PFR values is due to the adaptive learning process and variability in interference characteristics. As processing progresses, the algorithm optimizes and PFR values stabilize, indicating effective DSI suppression. Following DSI suppression, the proposed algorithm demonstrates a more pronounced suppression effect compared to traditional algorithms, achieving a suppression performance that is 1.4 dB higher than that of the LMS method. The Mean PFR values presented in Tab. 4 represent the overall average performance of each DSI suppression method across all segments processed in the simulation experiments. These values are calculated based on a sample size of 100 segments for each method, providing a comprehensive and statistically significant measure of performance.

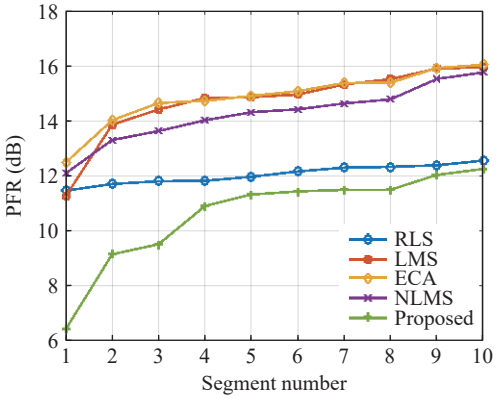

Fig. 11 PFR performance comparisons of proposed method, LMS, NLMS, RLS, ECA

Tab. 4 Mean PFR and runtimes for different DSI methods

Method	Mean PFR (dB)	Runtime (s)
RLS	12.05	25.94
NLMS	14.25	1.56
LMS	14.69	1.39
ECA	14.86	0.63
Proposed	10.60	1.05

Furthermore, the analysis incorporates the running times of each algorithm, providing a comprehensive perspective on performance. These tests were conducted using MATLAB 2018 on a Windows system powered by an Intel Xeon Gold 5 118 processor. The running times for the algorithms are detailed in Tab. 4. Although the proposed algorithm exhibits a longer running time compared to the traditional ECA method, it compensates for this with a superior suppression performance of 4.2 dB, demonstrating a significant advantage in terms of system resource efficiency.

5 Conclusion

This paper focuses on the suppression of DSI in PBR systems based on DVB-S and introduces a novel method for DSI suppression. Firstly, the received signal undergoes preprocessing, and then the signal from the reference channel and the surveillance channel is segmtioned with overlapping parts, which will help to improve the adaptive filter smoothness and improve the processing performance of the system. The segmented signals are then transformed using the FFT, and clutter is suppressed at each frequency point using filtering techniques. The processed signals are subsequently reconstructed by performing an IFFT to obtain the clutter suppressed echo signal.

Compared to traditional DSI suppression methods, the approach proposed in this paper shows advantages in terms of both computational efficiency and suppression effectiveness. The superior performance of this method is corroborated through simulation experiments involving both single and multiple target scenarios.

References:

[1] H. Griffiths and C. Baker, *An introduction to passive radar*, second edition, Artech, 2022.

[2] I. Pisciottano, D. Pastina, and D. Cristallini, "DVB-S based passive radar imaging of ship targets," in *2019 20th International Radar Symposium (IRS)*, Ulm, Germany, pp. 1-7, 2019.

[3] H. Nies, T. Mulic, F. Behner, S. Reuter, and I. Ihrke, "Ship tracking and imaging using DVB-S signals and a low-cost passive receiver system," in *15th European Conference on Synthetic Aperture Radar*, Munich, Germany, pp. 438-442, 2024.

[4] F. Colone,"DVB-T-based passive forward scatter radar: inherent limitations and enabling solutions," *IEEE Transactions on Aerospace and Electronic Systems*, vol. 57, no. 2, pp. 1084-1104, 2021.

[5] H. Zeng, J. Chen, P. Wang, W. Liu, X. Zhou, and W. Yang,"Moving target detection in multi-static GNSS-based passive radar based on multi-bernoulli filter," *Remote Sensing*, vol. 12, no. 21, pp. 3495, 2020.

[6] D. Pastina, F. Santi, F. Pieralice, M. Antoniou, and M. Cherniakov,"Passive radar imaging of ship targets with GNSS signals of opportunity," *IEEE Transactions on Geoscience and Remote Sensing*, vol. 59, no. 3, pp. 2627-2642, 2021.

[7] H. Zheng, S. Cheng, and M. Zhang, "Reference signal reconstruction for GPS-based passive radar based on software radio platform," in *2023 IEEE 6th Information Technology, Networking, Electronic and Automation Control Conference (ITNEC)*, Chongqing, China, pp. 732-736, 2023.

[8] C. Huang, Z. Li, M. Lou, X. Qiu, H. An, J. Wu, J. Yang, and W. Huang,"BeiDou-based passive radar vessel target detection: Method and experiment via long-time optimized integration," *Remote Sensing*, vol. 13, no. 19, pp. 3933, 2021.

[9] C. Zhang, S. Shi, S. Yan, and J. Gong,"Moving target detection and parameter estimation using BeiDou GEO satellites-based passive radar with short-time integration," *IEEE Journal of Selected Topics in Applied Earth Observations and Remote Sensing*, vol. 16, pp. 3959-3972, 2023.

[10] M. Horlbeck, J. Fiedelak, T. Kurin, B. Scheiner, R. Weigel, and F. Lurz, "Direct sampling receiver with an adjustable bandpass filter for use in passive radar with FM radio," in *2024 IEEE Radio and Wireless Symposium (RWS)*, San Antonio, TX, USA, pp. 102-104, 2024.

[11] R. Tao, H. Wu, and T. Shan,"Direct-path suppression by spatial filtering in digital television terrestrial broadcasting-based passive radar," *IET Radar, Sonar and Navigation*, vol. 4, no. 6, pp. 791-805, 2010.

[12] W. Ma, G. Tu, Z. Deng, X. Lu, Y. Ye, and Y. Li,"A novel wideband radar detector via Wiener filter," *Electronics Letters*, vol. 58, no. 13, pp. 505-507, 2022.

[13] M. Attalah, T. Laroussi, F. Gini, and M. Greco, "Fast block LMS algorithm for interference cancellation in DVB-T based passive bistatic radar," in *2017 5th International Conference on Electrical Engineering - Boumerdes (ICEE-B)*, Boumerdes, Algeria, pp. 1-5, 2017.

[14] Y. Xu, R. Tao, Y. Wang, and T. Shan,"Using LMS adaptive filter in direct wave cancellation," *Journal of Beijing Institute of Technology*, vol. 12, no. 4, pp. 425-427, 2003.

[15] Z. Yuan and X. Songtao, "Application of new LMS adaptive filtering algorithm with variable step size in adaptive echo cancellation," in *2017 IEEE 17th*

International Conference on Communication Technology (ICCT), Chengdu, China, pp. 1715-1719, 2017.

[16] J. Sui, J. Wang, J. Gao, and X. Fan, "A novel strong clutter suppression algorithm for airborne passive radar," in *2021 CIE International Conference on Radar (Radar)*, Haikou, Hainan, China, pp. 2791-2794, 2021.

[17] J. Sui, J. Wang, L. Zuo, and J. Gao,"Cascaded least square algorithm for strong clutter removal in airborne passive radar," *IEEE Transactions on Aerospace and Electronic Systems*, vol. 58, no. 1, pp. 679-696, 2022.

[18] D. Bismor,"Leaky partial update LMS algorithms in application to structural active noise control," *Sensors*, vol. 23, no. 3, pp. 1169, 2023.

[19] Y. Ma, T. Shan, Y. Zhang, M. Amin, R. Tao, and Y. Feng,"A novel two-dimensional sparse-weight NLMS filtering scheme for passive bistatic radar," *IEEE Geoscience and Remote Sensing Letters*, vol. 13, no. 5, pp. 676-680, 2016.

[20] Z. Yang, S. Ma, N. Liu, K. Chang, and X. Lyu,"A novel clutter suppression algorithm for low-slow-small targets detecting based on sparse adaptive filtering," *Journal of Beijing Institute of Technology*, vol. 33, no. 1, pp. 54-64, 2024.

[21] X. Bai, J. Han, J. Zhao, Y. Feng, and R. Tao, "Clutter cancellation in passive radar using batch-based CLEAN technique," *EURASIP Journal on Advances in Signal Processing*, vol. 63, pp.1-19, 2021.

[22] F. Colone, C. Palmarini, T. Martelli, and E. Tilli,"Sliding extensive cancellation algorithm for disturbance removal in passive radar," *IEEE Transactions on Aerospace and Electronic Systems*, vol. 52, no. 3, pp. 1309-1326, 2016.

[23] F. Colone, D. O'Hagan, P. Lombardo, and C. Baker,"A Multistage Processing Algorithm for Disturbance Removal and Target Detection in Passive Bistatic Radar," *IEEE Transactions on Aerospace and Electronic Systems*, vol. 45, no. 2, pp. 698-722, 2009.

[24] C. Palmarini, T. Martelli, F. Colone, and P. Lombardo, "Disturbance removal in passive radar via sliding extensive cancellation algorithm (ECA-S)," in *2015 IEEE Radar Conference*, Johannesburg, South Africa, pp. 162-167, 2015.

[25] X. Lyu, J. Xu, and J. Wang, "Clutter cancellation in passive radar from the perspective of maximum likelihood," in *2021 CIE International Conference on Radar (Radar)*, Haikou, Hainan, China, pp. 2808-2811, 2021.

[26] J. Garry, C. Baker, and G. Smith,"Evaluation of direct signal suppression for passive radar," *IEEE Transactions on Geoscience and Remote Sensing*, vol. 55, no. 7, pp. 3786-3799, 2017.

Jianyu He received his bachelor's degree from Hunan University of Science and Technology in 2022. He is currently a postgraduate student at the School of Communication and Information Engineering, Shanghai University, Shanghai, China. He is interested in passive bistatic radar signal processing.

Hongwen Yu received the B.S. and M.S. degrees in communication and information engineering from Shanghai University, Shanghai, China, in 2011 and 2014, respectively. He is currently pursuing the Ph.D. degree with the School of Electrical and Data Engineering, University of Technology Sydney, Ultimo, NSW, Australia, and Shanghai University. His current research interests include optimization methods for wireless communications and signal processing.

Zhichao Sheng received the Ph.D. degree in electrical engineering from the University of Technology Sydney, Sydney, NSW, Australia, in 2018. From 2018 to 2019, he was a Research Fellow with the School of Electronics, Electrical Engineering and Computer Science, Queen's University Belfast, Belfast, U.K. He is currently a Lecturer with Shanghai University, Shanghai, China. His research interests include optimization methods for wireless communication and signal processing.

Yong Fang received the Ph.D. degree in electronic engineering from the City University of Hong Kong, Hong Kong, in 1999. He is currently a Professor with the School of Communication and Information Engineering, Shanghai University, Shanghai, China. His research interests include communication signal processing, blind signal processing, and adaptive information systems.